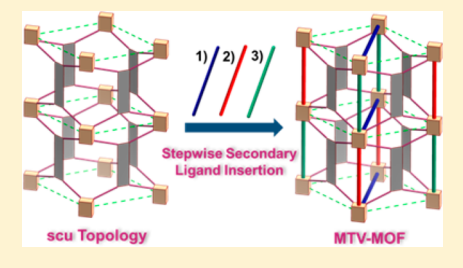


Topology-Guided Stepwise Insertion of Three Secondary Linkers in Zirconium Metal-Organic Frameworks

Xin Zhang,[†] Brandon L. Frey,[†] Yu-Sheng Chen,[‡] and Jian Zhang*,[†]

Supporting Information

ABSTRACT: We report a topology-guided, precise insertion of three distinct secondary linkers into a zirconium-based metal-organic framework, NPF-300. Constructed from a tetratopic linker L and Zr₆ cluster, NPP-300 exhibits a unique scu topology and certain flexibility along the crystallographic a axis, and in conjunction with the conformation change of the primary ligand, is able to accommodate the stepwise insertion of three different secondary linkers along the a and c axes. Size-matching and mechanic strain of the resulting framework are two important factors that determine the chemical stability of the inserted linkers. Secondary linker insertion in NPF-300 significantly enables not only its porosity but



also potentials to install up to three different functional groups for the construction of multivariate MOFs with homogeneity.

■ INTRODUCTION

Metal-organic frameworks (MOFs) are inorganic-organic hybrid materials constructed via the self-assembly of judiciously selected organic and inorganic building blocks. As an emerging class of nanoporous solids with modular nature, MOFs exhibit predictable topology, tailorable porosity, and tunable functionality, and are suited for a wide range of applications including gas storage, catalysis, and sensing, to name a few.³ To further broaden the utility of MOFs, it is important to increase the complexity and/or introduce synergistic effects without compromising their ordered structure. One synthetic strategy is to introduce "heterogeneity within order",5 a concept developed by Yaghi and co-workers, who have demonstrated the facile incorporation of up to eight distinct linkers with similar length but different functionalities into one single framework.° Despite the lack of knowledge of the exact location of each functional group due to the disordered distribution within the framework, the resulted multivariate MOFs (MTV-MOFs) can exhibit enhanced properties in gas adsorption and multifunctional heterogeneous catalysis compared to their prototypic framework.

Another strategy to achieve a higher degree of functionality of MOFs is to place multiple topologically distinct linkers at the precise positions in the crystalline lattice, i.e., to construct MTV-MOFs with homogeneity. Although this objective can be achieved via a one-pot, mixed linker strategy where distinct linkers are simultaneously incorporated into one framework, the postsynthetic stepwise ligand insertion 10b appears to be a more reliable approach. 10 Recently, the Zhou group and the Su group utilizes the sequential linker installation (SLI) (or postsynthetic variable spacer installation, PVSI) to insert two different secondary linkers (SLs) in a stepwise fashion into a class of elastic PCN-700 (or LIFM-28) series. 11 Despite the

exciting progress, incorporating three distinct SLs within one framework remains a challenge and, to the best of our knowledge, has not been reported.

Herein, we disclose the construction of a new series of MTV-MOFs with homogeneity via a topology-guided stepwise insertion of three different SLs within a prototypic Zr-MOF (NPF-300, NPF = Nebraska Porous Framework) (Figure 1). Assembled from a planar tetratopic primary linker L and eightconnected Zr₆O₄(OH)₈(H₂O)₄ clusters, NPF-300 exhibits the unique scu topology. Upon the removal of the OH⁻/H₂O ligands of the Zr₆ clusters, a secondary linear dicarboxylate linker with an appropriate length can be first inserted into the framework along the a axis (Figure 1c). Next, the in-plane and out-of-plane bending flexibility of the primary linker L enables the *stepwise* insertion of two other SLs along the *c* axis. Detailed stability evaluations reveal that the size-matching and the framework strain are two important factors that dictate the interplay between the thermodynamics and kinetics of the linker insertion and dissociation. Overall, this topology-guided secondary linker insertion enables the permanent porosity of NPF-300 and the potentials for the installation of multiple functionalities in a new prototype of MTV-MOFs.

RESULTS AND DISCUSSION

Tetratopic ligand H₄L was synthesized via the typical Suzuki, Sonogashira, and Glaser coupling followed by saponification in basic aqueous solution (see Supporting Information, SI-2, for detailed procedure). Light-yellow crystals of NPF-300 were obtained via a solvothermal reaction of ZrCl₄ with H₄L in dimethylformamide (DMF):dimethylacetamide (DEF) (v:v =

Received: April 22, 2018 Published: May 28, 2018



Department of Chemistry, University of Nebraska—Lincoln, Lincoln, Nebraska 68588, United States

[‡]ChemMatCARS, Center for Advanced Radiation Sources, The University of Chicago, 9700 South Cass Avenue, Argonne, Illinois 60439, United States

Journal of the American Chemical Society

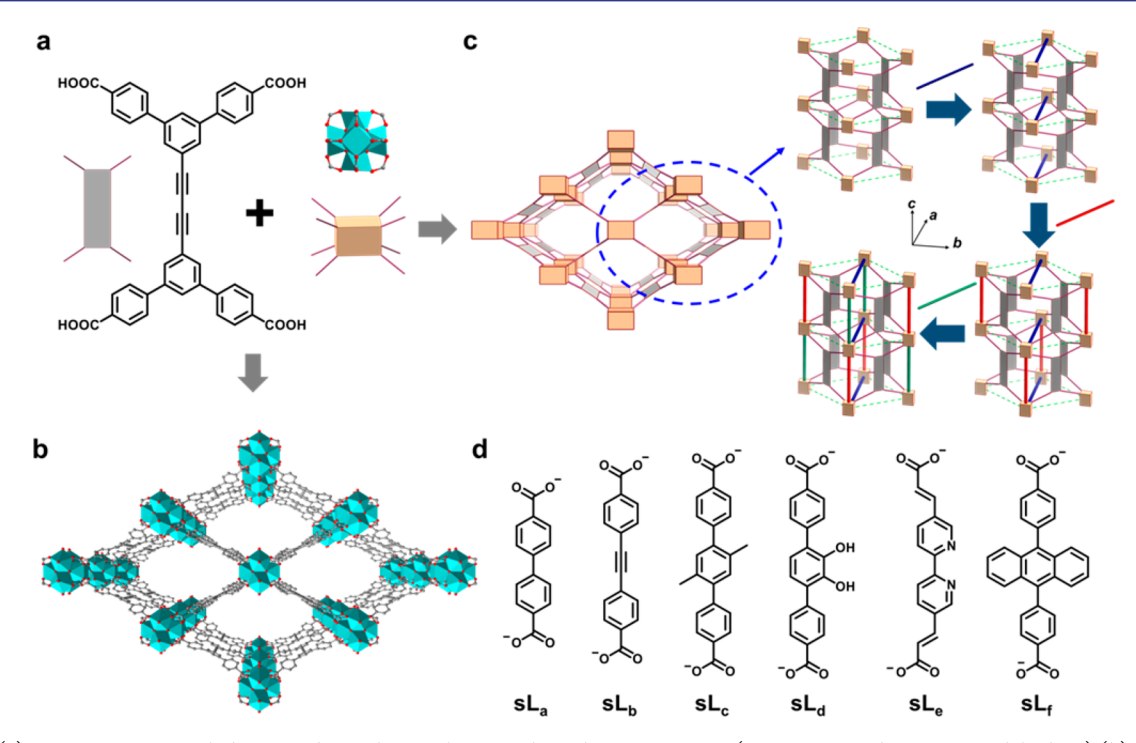


Figure 1. (a) Primary tetratopic linker L and Zr₆ cluster, their topological representation (C, gray; O, red, Zr, cyan polyhedron).(b) Structure of NPF-300. (c) The augmented scu and schematic illustration of the stepwise insertion of three SLs. (d) Structure of the six SLs used in this study.

8:1) with benzoic acid as the modulating agent at 120 $^{\circ}\text{C}$ for 48 h. Single-crystal X-ray diffraction (sc-XRD) study at room temperature reveals that NPF-300 crystallizes in the orthorhombic crystal system with a Cmmm space group. Each tetratopic ligand L is connected to four Zr₆ clusters that are organized in a C-centered orthorhombic arrangement (Figure S16, SI). Each Zr₆ cluster is coordinated with eight L linkers with four above and four below the equatorial plane and eight terminal H₂O/OH⁻ groups in the equatorial plane (Figure S17), which gives the overall formula of NPF-300 as $Zr_6O_4(OH)_8(H_2O)_4L_2$. The combination of the large size of linker L and the unique scu topology¹² results in four large 1D open channels in NPF-300, namely, rhombic channels of with a size of 27×15 Å along the c axis, rhombic channels with a size of 9×13 Å along the b axis, rhombic channels of with a size of 8×9 Å and hexagonal channels with a diameter of 15 Å along a axis (Figures S13-S15).

The powder XRD pattern of the solvated NPF-300 exhibits an excellent agreement with the simulation, confirms the bulk purity of the material (Figure 2a). Interestingly, a second sc-XRD study of NPF-300 at 110 K (designated as NPF-300-LT) reveals a 10% decrease of the crystallographic a axis and 2.2% and 1% increase of the b and c axes, respectively, as well as an overall 7.0% decrease of unit cell volume (Figure 2b, Table S1). A Hf-MOF (NPF-300(Hf)) also exhibits similar cell parameters at 110 K (Table S1). A close examination of the crystal structure shows that the temperature-dependent deformation is mainly due to the subtle change of the conformation of ligand L: the dihedral angle between the terminal and the center phenyl rings of L in NPF-300 and NPF-300-LT is 42.2° and 39.6°, respectively (Figure S18), which results in a small flexibility of NPF-300 crystals along the a axis. Zr-MOFs consisting 8-connected Zr₆O₄(OH)₈(H₂O)₄ clusters are ideal platforms for SL insertion via the replacement of OH⁻/H₂O groups on the clusters. ^{11,13} Encouraged by the small flexibility of NPF-300 along the a axis, we first tested the possibility to

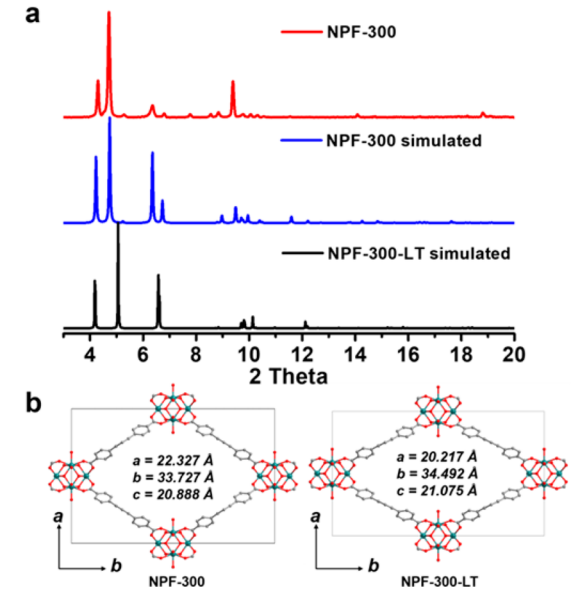
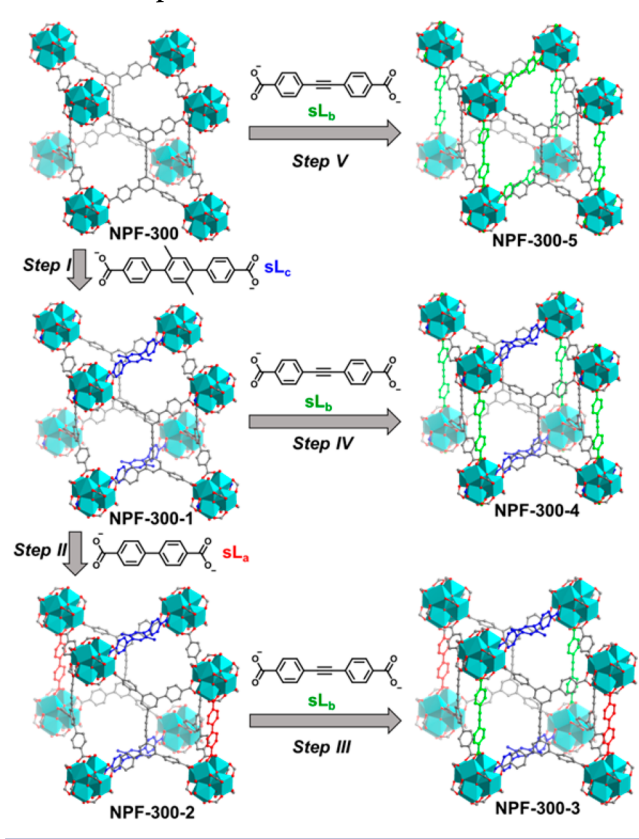


Figure 2. (a) Experimental and simulated powder XRD patterns of NPF-300 and NPF-300-LT. (b) Structure of NPF-300 and NPF-300-LT viewed from the c axis.

insert linker \mathbf{sL}_{c} as the first SL since its length (15.4 Å) is close to the O-O distance between the adjacent Zr₆ clusters along the a axis (14.5 Å) (Scheme 1, Step I). Briefly, NPF-300 crystals were placed in the solution of sL_c in DMF at 60 °C for 24 h, and the resulting crystalline material, termed as NPF-300−1, crystallizes in the same *Cmmm* space group as NPF-300 and displays the presence of sL_c at the expected position. In NPF-300-1, each Zr₆ cluster is 10-connected to eight primary L and two secondary sL_c linkers, with the overall composition of $Zr_6O_4(OH)_6(H_2O)_2(L)_2(sL_c)$, which is confirmed by ¹H NMR of a digested sample (vide infra, Table 1 and Figure S5).

Scheme 1. Stepwise Insertion of SL in NPF-300



The powder XRD patterns reveal the crystallinity of the bulk material and confirm the nature of single-crystal-to-single-crystal transformation (Figure S21).

Upon the insertion of first SL sL_c, the O-O distance between the adjacent 10-connected Zr₆ clusters along the c axis is 12.8 Å, close to the length of the linear ditopic linker sLa (11.3 Å). We then used sL_a as the second SL for the insertion in NPF-300-1 using a similar method and successfully obtained the single crystals of NPF-300-2 (Scheme 1, Step II). NPF-300-2 crystallizes in the *Immm* space group, and its unit cell is nearly doubled compared to NPF-300 and NPF-300−1 due to the alternating arrangement of sL_a between the adjacent Zr₆ clusters along the c axis. Thus, each Zr₆ cluster is 11-connected to eight primary L, two sL_{c} , and one sL_{a} , with the overall composition of $Zr_6O_4(OH)_5(H_2O)(L)_2(sL_c)(sL_a)_{1/2}$ which was confirmed by ¹H NMR (vide infra, Table 1 and Figure S6).14 Remarkably, the O-O distance between the adjacent 11-connected Zr₆ clusters in NPF-300-2 along the c axis is 14.5 Å, suitable for the insertion of a third SL sL, with a

length of 13.8 Å, which yielded NPF-300–3 (Scheme 1, Step III). The space group of NPF-300–3 remains as *Immm*, and each Zr_6 cluster is now 12-connected to eight primary L and two sL_{c} one sL_a , and one sL_b with the overall composition of $Zr_6O_4(OH)_4(L)_2(sL_c)(sL_a)_{1/2}(sL_b)_{1/2}$, which is confirmed by ¹H NMR (vide infra, Table 1 and Figure S7). Powder XRD analysis also confirms the bulk crystallinity of NPF-300–2 and NPF-300–3 (Figures S22 and S23).

The successful stepwise insertion of three distinct SLs in NPF-300 benefits from the unique scu topology and relatively large size of the primary tetratopic ligand L that offers unique spaces to accommodate linker insertion. More importantly, the flexibility of the phenyl–alkynyl–alkynyl–phenyl backbone of the primary ligand plays an important role. A close comparison of molecular geometry of L in NPF-300–1 and NPF-300–2 reveals a small but critical out-of-plane and in-plane distortion, indicated by the change of the dihedral angle between two central phenyl planes from 0° to 11.1° and the change of symmetry from C_{2h} to C_s (Figure 3). Such distortion is caused by the half occupancy of \mathbf{sL}_a within the empty space along the c axis and offers the possibility of the third SL insertion.

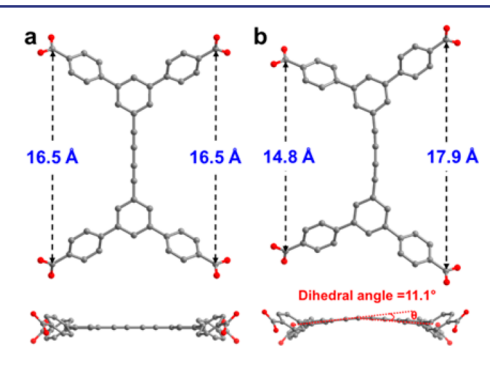


Figure 3. Top and side views of the conformation of primary linker L in NPF-300-1 (a) and NPF-300-2 (b) showing the in-plane and out-of-plane distortion.

It should be noted that the length of SL and the sequence of insertion is essential to a successful insertion. The For instance, inserting a slightly longer linker $\mathbf{sL_b}$ instead of $\mathbf{sL_a}$ as the second SL into NPF-300–1 results in its complete occupancy along the c axis (Scheme 1, Step IV). The resulting single crystal material, termed as NPF-300–4, has a composition of $\mathrm{Zr_6O_4(OH)_4(L)_2(sL_a)(sL_b)}$. Moreover, the attempted insertion of $\mathbf{sL_b}$ first along the c axis in NPF-300 was not successful and instead led to the simultaneous linker insertion along both a and c axes and yielded NPF-300–5, a framework with the overall composition of $\mathrm{Zr_6O_4(OH)_4(L)_2(sL_b)_2}$ (Scheme 1, Step

Table 1. Chemical Stability of NPF-300 MTV-MOFs

	molar ratio	theoretical value	as prepared ^a	water ^{a,b}	$pH = 11^{a,c}$	$pH = 1^{a,d}$
NPF-300-1	$L:sL_c$	2:1	2.00:1.00	2.00:1.00	2.00:1.00	2.00:1.04
NPF-300-2	$L:sL_c:sL_a$	2:1:0.5	2.00:1.10:0.92 ^e	2.00:1.04:0.79 ^e	2.00:1.07:0.76 ^e	2.00:0.71:0.61 ^e
NPF-300-3	$L:sL_c:sL_a:sL_b$	2:1:0.5:0.5	2.00:0.97:0.52:0.58	2.00:1.00:0.49:0.57	2.00:1.01:0.46:0.56	2.00:0.67:0.10:0.27
NPF-300-4	$L:sL_c:sL_b$	2:1:1	2.00:1.04:1.05	2.00:1.04:0.98	2.00:1.03:0.93	2.00:0.16:0.43
NPF-300-5	$L:sL_b$	2:2	2.00:1.99	2.00:1.51	2.00:1.16	2.00:0.49

^aMolar ratios were calculated by comparing the characteristic peaks of samples digested in K₃PO₄ solution in ¹H NMR, as shown in Figures S41–S44. A standard deviation of 10% was estimated based on three measurements. ^bSamples soaked in water. ^cSamples soaked in solutions with pH values adjusted by HCl. ^dSamples soaked in solutions with pH values adjusted by NaOH. ^eThe values are higher than the expected value (0.5), indicating the additional binding of sL_a along the *c* axis, most likely via one of the carboxyl groups.

Table 2. Porosity Parameters, Density, and N2 Uptakes for NPF-300 MTV-MOFs

	NPF-300	NPF-300-1	NPF-300-2	NPF-300-3	NPF-300-4	NPF-300-5
$SA_{BET} (m^2 g^{-1})^a$	419	3276	2963	2750	2978	2565
$SA_V (m^2 mL^{-1})$	109	1657	1564	1529	1611	1449
$V_{\rm p} \ ({\rm cm}^3 \ {\rm g}^{-1})$	0.26	1.63	1.18	1.11	1.19	1.03
$D_{\rm c}~({\rm g~cm}^{-3})$	0.456	0.512	0.528	0.556	0.541	0.565
N ₂ uptake ^c	121	853	763	715	771	669

"Surface area (m² g⁻¹) calculated from N₂ adsorption at 77 K based on the BET model. "One bar; unit of gas uptake, cm³ g⁻¹.

V). This is likely due to the intrinsic flexibility of NPF-300 for accommodation of $\mathbf{sL_b}$ (13.8 Å) in all three positions. Similarly, ¹H NMR and powder XRD analysis confirmed the composition and bulk crystallinity. (Table 1 and Figures S24 and S25).

With the MTV-MOF materials in hand, we next assessed their thermal stability via thermogravimetric analysis. All MOFs exhibit a high decomposition temperature around 450–500 °C, indicating their good thermal stability at elevated temperature (Figure S49). Excellent crystallinity also remains after treatment in H₂O, basic (pH = 11), and acidic (pH = 1) conditions (Figure S40). However, the chemical stability of NPF-300 series is better quantified by digestion analysis. This is because the partial or complete dissociation of SLs in MTV-MOFs does not necessarily result in a change of crystallinity. Indeed, upon digestion, ¹H NMR spectra revealed the dissociation of SLs to various extent. Using the primary ligand L as the internal reference, the relative molar ratio before and after the treatments was quantified and summarized in Table 1.

First, among the five MTV-MOFs, NPF-300-1 exhibits the highest stability as indicated by the consistent L:sLc molar ratio of ~2:1 in water, basic, and acidic conditions (Table 1). This can be attributed to the good size-matching of sL_c and the distance between the adjacent Zr₆ clusters along the a axis. Such thermodynamic stability is also indicated by the insignificant change of powder XRD patterns (Figure S40) and unit cell volume (~0.4% increase) after the ligand insertion (Table S1). Second, the overall stability of other four MTV-MOFs follows the trend: water > pH = 11 > pH = 1. Except NPF-300-5, all MTV-MOFs exhibit impressive stability in water and basic conditions. At the same time, the chemical stability is roughly in correlation to the deviation of the lattice parameters from NPF-300-1. For instance, compared to NPF-300-1, the unit cell volume of NPF-300-4 and NPF-300-5 increases by 2.6% and decreases by 4.7%, respectively (Table S1). Accordingly, the inserted SLs in these two MOFs are more kinetically controlled and significantly dissociate especially in acidic solution (Table 1). Lastly, the dissociation of sL_a and sL_b also causes the simultaneous detachment of sL_c. Specifically, in contrast to its high stability in NPF-300-1, sLc partially dissociates in NPF-300-2 and NPF-300-3 in acidic condition (e.g., $L:sL_c$ ratio decreases from 2.00:1.04 to 2.00:0.71 and 2.00:0.67, respectively).

Overall, in contrast to PCN-700 and LIFM-28 series where the dynamic twisting of the primary ligand plays an essential role in the insertion and water-promoted, facile dissociation of SLs, ^{11d} the ligand insertion in NPF-300 series is more based on size-matching, which exerts less mechanical strain on the primary framework and results in the significantly improved stability of NPF-300 series in aqueous solutions. In particular, with the insertion of a size-matched linker and the least amount of strain, NPF-300–1 exhibits excellent resistance toward acidic and basic conditions.

We next determined the porosity parameters of NPF-300 series. Unlike some other Zr-MOFs with **scu** topology, NPF-300 loses its crystallinity upon desolvation (Figure S20). ^{12c,f-i,15} Even after the activation by supercritical CO₂ exchange, ¹⁶ it only exhibits a low BET surface area (SA_{BET}) of 419 m²/g (Table 2 and Figure S29). To our delight, the insertion of SLs enables the permanent porosity of all MTV-MOFs. In particular, NPF-300-1, with sL_c inserted along the a axis exhibits the highest SA_{BET} of 3236 m²/g, an increase more than seven times (Table 2 and Figure S30). The insertion additional linkers such as sL_a (in NPF-300-2) and sL_b+sL_a (in NPF-300-3), albeit the retention of permanent porosity, however results in a slight decrease of SA_{RET} due to their occupation of the free space inside the MOF cavity (Table 2 and Figures S31 and S32). Among the three MTV-MOFs with full insertion of SLs, NPF-300–4 exhibits the highest SA_{BET} (2978 m²/g, 16.1% higher than NPF-300-5), which is correlated to its largest cell volume (7.7% larger than NPF-300-5) (Table 2 and Figures S33 and S34).

It should be pointed out that the regioselectivity for $\mathbf{sL_b}$ insertion in forming NPF-300–5 is poor. It is observed that, as the amount of $\mathbf{sL_b}$ used in the linker insertion in NPF-300–5 increases, the SA_{BET} of the resulting material increases (Figure 4). Since the realization of surface area is closely related to the

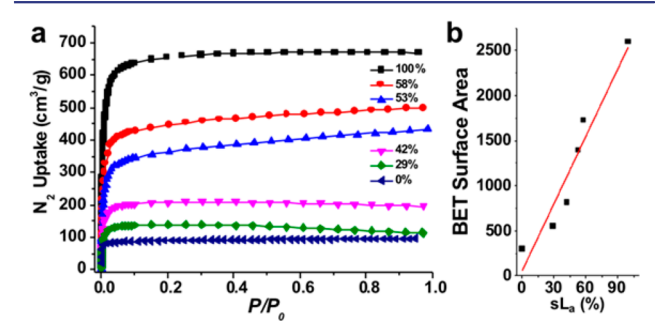


Figure 4. (a) N_2 gas adsorption isotherm and (b) SA_{BET} for NPF-300 with different amount of inserted linker sL_b . The percentage was calculated using the experimentally determined value vs the theoretical amount assuming complete insertion was obtained.

linker insertion along the a axis, the pseudo linear correlation between the SA_{BET} and the ratio of inserted ligand (determined by ^{1}H NMR after digestion) strongly suggests that insertion along both a and c axis occurs simultaneously. In addition, powder XRD patterns also demonstrate the gradual change of unit cell parameters as the ligand insertion proceeds (Figure S38).

Having established their permanent porosity, we further tested the potential utility of NPF-300 series in gas storage by evaluating the uptake capacity for H₂, CO₂, and CH₄. Thanks to their permanent porosity, all five MTV-MOFs exhibit significantly better performance compared to the collapsed

prototypic NPF-300 (Figures S46-S48, Table S2). In particular, NPF-300-1 shows the highest uptake for H₂ (1.7 wt % at 77 K), CO₂ (15 wt % at 273 K), and CH₄ (1.4 wt % at 273 K), due to its largest surface area, pore volume, and lowest density (Table 2). It is interesting that at low pressure (0-40)mmHg), the CO₂ adsorption of NPF-300-2 is the highest among all (Figure S48), which is likely due to the strong interaction between CO2 and the extra dangling sL2 we proposed to account for its high ratio. It is foreseeable that the current moderate performance can be readily improved via further functionalization of the secondary linkers such as sL. and sL₂ to achieve enhanced gas adsorption capability as well as selectivity. 11b,e Other functional SLs with metal chelating group can also be incorporated in NPF-300. For example, we were able to insert catechol-17 and bipyridine-based 18 SLs (i.e., sLd and sL_e) and obtained the corresponding NPF-300-6 and -7, respectively (Figures S10 and S11 and Table S1). The similar length of sL_d and sL_e to sL_c enables insertion along the a axis as such in NPF-300−1. Similarly, sL_t, a secondary linker derived from DPA (9,10-diphenylanthracene) can also be inserted and forming NPF-300-8 (Figure S12 and Table S1), which can be potentially utilized for heterogeneous photophysical and photochemical applications.19

In summary, we have synthesized a new class of prototypic MTV-MOFs based on the (4,8)-connected NPF-300 series using topology as a guidance. The unique positions of eightconnected Zr₆ clusters in the scu network and the flexibility of the tetratopic primary linker L enable the precise insertion of up to three different distinct secondary linkers along the a and c axis via stepwise, single-crystal-to-single-crystal transformation. We have revealed that the size-matching of the inserted linker and the framework strain are two important factors that govern the overall stability of MTV-MOFs. To the best of our knowledge, NPF-300 represents the first structure prototype that has the capability to introduce three distinct functional groups into a single MOF in a crystallographically ordered fashion. It is our expectation that NPF-300 can be used to build multifunctional MOF materials for a wide range of applications including gas storage/separation and synergistic/cooperative catalysis.

ASSOCIATED CONTENT

S Supporting Information

The Supporting Information is available free of charge on the ACS Publications website at DOI: 10.1021/jacs.8b04277.

Materials, general experimental procedures, synthesis of NPF-300 series, and characterizations of compounds (PDF)

Crystallographic data (CIF)

Crystallographic data (CIF) Crystallographic data (CIF)

Crystallographic data (CIF)

AUTHOR INFORMATION

Corresponding Author

*jzhang3@unl.edu

ORCID ®

Jian Zhang: 0000-0003-0274-0814

The authors declare no competing financial interest.

ACKNOWLEDGMENTS

J.Z. acknowledges a National Science Foundation CAREER ward (DMR-1554918) for support of this research. This work is also partially supported by NSF/CBET-1706632. Chem-MatCARS Sector 15 is principally supported by the Divisions of Chemistry (CHE) and Materials Research (DMR), National Science Foundation, under grant number NSF/CHE-1346572. Use of the APS, an Office of Science User Facility operated for the U.S. DOE Office of Science by ANL, was supported under Contract No. DE-AC02-06CH11357.

REFERENCES

- (1) (a) Tranchemontagne, D. J.; Mendoza-Cortes, J. L.; O'Keeffe, M.; Yaghi, O. M. Chem. Soc. Rev. 2009, 38, 1257-1283. (b) O'Keeffe, M.; Yaghi, O. M. Chem. Rev. 2012, 112, 675-702. (c) Li, M.; Li, D.; O'Keeffe, M.; Yaghi, O. M. Chem. Rev. 2014, 114, 1343-1370. (d) Schoedel, A.; Li, M.; Li, D.; O'Keeffe, M.; Yaghi, O. M. Chem. Rev. 2016, 116, 12466-12535.
- (2) (a) Yaghi, O. M.; O'Keeffe, M.; Ockwig, N. W.; Chae, H. K.; Eddaoudi, M.; Kim, J. Nature 2003, 423, 705-714. (b) Kitagawa, S.; Kitaura, R.; Noro, S. Angew. Chem., Int. Ed. 2004, 43, 2334-2375. (c) Ferey, G. Chem. Soc. Rev. 2008, 37, 191-214.
- (3) (a) Long, J. R.; Yaghi, O. M. Chem. Soc. Rev. 2009, 38, 1213-1214. (b) Zhou, H. C.; Long, J. R.; Yaghi, O. M. Chem. Rev. 2012, 112, 673-674. (c) Furukawa, H.; Cordova, K. E.; O'Keeffe, M.; Yaghi, O. M. Science 2013, 341, 1230444. (d) Wang, C.; Liu, D.; Lin, W. J. Am. Chem. Soc. 2013, 135, 13222-13234. (e) Zhou, H. C.; Kitagawa, S. Chem. Soc. Rev. 2014, 43, 5415-5418. (f) Lustig, W. P.; Mukherjee, S.; Rudd, N. D.; Desai, A. V.; Li, J.; Ghosh, S. K. Chem. Soc. Rev. 2017, 46, 3242-3285. (g) Yang, Q.; Xu, Q.; Jiang, H.-L. Chem. Soc. Rev. 2017, 46, 4774-4808.
- (4) (a) Burrows, A. D. CrystEngComm 2011, 13, 3623-3642. (b) Liu, C.; Luo, T. Y.; Feura, E. S.; Zhang, C.; Rosi, N. L. J. Am. Chem. Soc. 2015, 137, 10508-10511. (c) Zhao, X.; Bu, X.; Nguyen, E. T.; Zhai, Q. G.; Mao, C.; Feng, P. J. Am. Chem. Soc. 2016, 138, 15102-15105. (d) Zhai, Q. G.; Bu, X.; Zhao, X.; Li, D. S.; Feng, P. Acc. Chem. Res. 2017, 50, 407-417.
- (5) Furukawa, H.; Muller, U.; Yaghi, O. M. Angew. Chem., Int. Ed. 2015, 54, 3417-3430.
- (6) (a) Deng, H.; Doonan, C. J.; Furukawa, H.; Ferreira, R. B.; Towne, J.; Knobler, C. B.; Wang, B.; Yaghi, O. M. Science 2010, 327, 846-850. (b) Kong, X.; Deng, H.; Yan, F.; Kim, J.; Swisher, J. A.; Smit, B.; Yaghi, O. M.; Reimer, J. A. Science 2013, 341, 882-885.
- (7) (a) Szilágyi, P. Á.; Weinrauch, I.; Oh, H.; Hirscher, M.; Juan-Alcañiz, J.; Serra-Crespo, P.; de Respinis, M.; Trześniewski, B. J.; Kapteijn, F.; Geerlings, H.; Gascon, J.; Dam, B.; Grzech, A.; van de Krol, R.; Geerlings, H. J. Phys. Chem. C 2014, 118, 19572-19579. (b) Zhang, Y. B.; Furukawa, H.; Ko, N.; Nie, W.; Park, H. J.; Okajima, S.; Cordova, K. E.; Deng, H.; Kim, J.; Yaghi, O. M. J. Am. Chem. Soc. 2015, 137, 2641-2650. (c) Naeem, A.; Ting, V. P.; Hintermair, U.; Tian, M.; Telford, R.; Halim, S.; Nowell, H.; Holynska, M.; Teat, S. J.; Scowen, I. J.; Nayak, S. Chem. Commun. 2016, 52, 7826-7829.
- (8) (a) Liu, Q.; Cong, H.; Deng, H. J. Am. Chem. Soc. 2016, 138, 13822-13825. (b) Fracaroli, A. M.; Siman, P.; Nagib, D. A.; Suzuki, M.; Furukawa, H.; Toste, F. D.; Yaghi, O. M. J. Am. Chem. Soc. 2016, 138, 8352-8355. (c) Xia, Q.; Li, Z.; Tan, C.; Liu, Y.; Gong, W.; Cui, Y. J. Am. Chem. Soc. 2017, 139, 8259-8266.

- (9) (a) Kitaura, R.; Fujimoto, K.; Noro, S.-i.; Kondo, M.; Kitagawa, S. Angew. Chem., Int. Ed. 2002, 41, 133-135. (b) Dybtsev, D. N.; Chun, H.; Kim, K. Angew. Chem., Int. Ed. 2004, 43, 5033-5036. (c) Ma, B. Q.; Mulfort, K. L.; Hupp, J. T. Inorg. Chem. 2005, 44, 4912-4914. (d) Koh, K.; Wong-Foy, A. G.; Matzger, A. J. Angew. Chem., Int. Ed. 2008, 47, 677-680. (e) Doonan, C. J.; Morris, W.; Furukawa, H.; Yaghi, O. M. J. Am. Chem. Soc. 2009, 131, 9492-9493. (f) Klein, N.; Senkovska, I.; Gedrich, K.; Stoeck, U.; Henschel, A.; Mueller, U.; Kaskel, S. Angew. Chem., Int. Ed. 2009, 48, 9954-9957. (g) Fukushima, T.; Horike, S.; Inubushi, Y.; Nakagawa, K.; Kubota, Y.; Takata, M.; Kitagawa, S. Angew. Chem., Int. Ed. 2010, 49, 4820-4824. (h) Furukawa, H.; Ko, N.; Go, Y. B.; Aratani, N.; Choi, S. B.; Choi, E.; Yazaydin, A. O.; Snurr, R. Q.; O'Keeffe, M.; Kim, J.; Yaghi, O. M. Science 2010, 329, 424-428. (i) Burnett, B. J.; Barron, P. M.; Hu, C.; Choe, W. J. Am. Chem. Soc. 2011, 133, 9984-9987. (j) Chevreau, H.; Devic, T.; Salles, F.; Maurin, G.; Stock, N.; Serre, C. Angew. Chem., Int. Ed. 2013, 52, 5056-5060. (k) Liu, L.; Konstas, K.; Hill, M. R.; Telfer, S. G. J. Am. Chem. Soc. 2013, 135, 17731-17734.
- (10) (a) Kapustin, E. A.; Lee, S.; Alshammari, A. S.; Yaghi, O. M. ACS Cent. Sci. 2017, 3, 662–667. (b) Deria, P.; Mondloch, J. E.; Tylianakis, E.; Ghosh, P.; Bury, W.; Snurr, R. Q.; Hupp, J. T.; Farha, O. K. J. Am. Chem. Soc. 2013, 135, 16801–16804. (c) Deria, P.; Bury, W.; Hupp, J. T.; Farha, O. K. Chem. Commun. 2014, 50, 1965–1968. (d) Deria, P.; Bury, W.; Hod, I.; Kung, C. W.; Karagiaridi, O.; Hupp, J. T.; Farha, O. K. Inorg. Chem. 2015, 54, 2185–2192. (e) Li, T.; Kozlowski, M. T.; Doud, E. A.; Blakely, M. N.; Rosi, N. L. J. Am. Chem. Soc. 2013, 135, 11688–11691.
- (11) (a) Yuan, S.; Lu, W.; Chen, Y. P.; Zhang, Q.; Liu, T. F.; Feng, D.; Wang, X.; Qin, J.; Zhou, H. C. J. Am. Chem. Soc. 2015, 137, 3177—3180. (b) Yuan, S.; Chen, Y. P.; Qin, J. S.; Lu, W.; Zou, L.; Zhang, Q.; Wang, X.; Sun, X.; Zhou, H. C. J. Am. Chem. Soc. 2016, 138, 8912—8919. (c) Yuan, S.; Zou, L.; Li, H.; Chen, Y. P.; Qin, J.; Zhang, Q.; Lu, W.; Hall, M. B.; Zhou, H. C. Angew. Chem., Int. Ed. 2016, 55, 10776—10780. (d) Chen, C. X.; Wei, Z.; Jiang, J. J.; Fan, Y. Z.; Zheng, S. P.; Cao, C. C.; Li, Y. H.; Fenske, D.; Su, C. Y. Angew. Chem., Int. Ed. 2016, 55, 9932—9936. (e) Chen, C. X.; Wei, Z. W.; Jiang, J. J.; Zheng, S. P.; Wang, H. P.; Qiu, Q. F.; Cao, C. C.; Fenske, D.; Su, C. Y. J. Am. Chem. Soc. 2017, 139, 6034—6037.
- (12) (a) Kung, C.-W.; Wang, T. C.; Mondloch, J. E.; Fairen-Jimenez, D.; Gardner, D. M.; Bury, W.; Klingsporn, J. M.; Barnes, J. C.; Van Duyne, R.; Stoddart, J. F.; Wasielewski, M. R.; Farha, O. K.; Hupp, J. T. Chem. Mater. 2013, 25, 5012-5017. (b) Gomez-Gualdron, D. A.; Gutov, O. V.; Krungleviciute, V.; Borah, B.; Mondloch, J. E.; Hupp, J. T.; Yildirim, T.; Farha, O. K.; Snurr, R. Q. Chem. Mater. 2014, 26, 5632-5639. (c) Deria, P.; Gomez-Gualdron, D. A.; Hod, I.; Snurr, R. Q.; Hupp, J. T.; Farha, O. K. J. Am. Chem. Soc. 2016, 138, 14449-14457. (d) Lammert, M.; Reinsch, H.; Murray, C. A.; Wharmby, M. T.; Terraschke, H.; Stock, N. Dalton Trans. 2016, 45, 18822-18826. (e) Xu, L.; Luo, Y. P.; Sun, L.; Xu, Y.; Cai, Z. S.; Fang, M.; Yuan, R. X.; Du, H. B. Chem. - Eur. J. 2016, 22, 6268-6276. (f) Pang, J.; Yuan, S.; Qin, J.; Liu, C.; Lollar, C.; Wu, M.; Yuan, D.; Zhou, H. C.; Hong, M. J. Am. Chem. Soc. 2017, 139, 16939-16945. (g) Pang, J.; Yuan, S.; Du, D.; Lollar, C.; Zhang, L.; Wu, M.; Yuan, D.; Zhou, H. C.; Hong, M. Angew. Chem., Int. Ed. 2017, 56, 14622-14626. (h) Deria, P.; Yu, J.; Smith, T.; Balaraman, R. P. J. Am. Chem. Soc. 2017, 139, 5973-5983. (i) Noh, H.; Kung, C.-W.; Islamoglu, T.; Peters, A. W.; Liao, Y.; Li, P.; Garibay, S. J.; Zhang, X.; DeStefano, M. R.; Hupp, J. T.; Farha, O. K. Chem. Mater. 2018, 30, 2193-2197. (j) Deria, P.; Yu, J.; Balaraman, R. P.; Mashni, J.; White, S. N. Chem. Commun. 2016, 52, 13031-13034. (13) (a) Li, P.; Moon, S. Y.; Guelta, M. A.; Harvey, S. P.; Hupp, J. T.; Farha, O. K. J. Am. Chem. Soc. 2016, 138, 8052-8055. (b) Noh, H.; Cui, Y.; Peters, A. W.; Pahls, D. R.; Ortuno, M. A.; Vermeulen, N. A.; Cramer, C. J.; Gagliardi, L.; Hupp, J. T.; Farha, O. K. J. Am. Chem. Soc. 2016, 138, 14720-14726. (c) Ikuno, T.; Zheng, J.; Vjunov, A.; Sanchez-Sanchez, M.; Ortuno, M. A.; Pahls, D. R.; Fulton, J. L.; Camaioni, D. M.; Li, Z.; Ray, D.; Mehdi, B. L.; Browning, N. D.; Farha, O. K.; Hupp, J. T.; Cramer, C. J.; Gagliardi, L.; Lercher, J. A. J. Am. Chem. Soc. 2017, 139, 10294-10301.

- (14) The molar ratio of inserted sL_a is systematically higher than the expected value, which indicates the partial coordination to Zr cluster via one of the two carboxyl groups.
- (15) Goswami, S.; Ray, D.; Otake, K.-i.; Kung, C.-W.; Garibay, S. J.; Islamoglu, T.; Atilgan, A.; Cui, Y.; Cramer, C. J.; Farha, O. K.; Hupp, J. T. Chem. Sci. **2018**, *9*, 4477–4482.
- (16) Nelson, A. P.; Farha, O. K.; Mulfort, K. L.; Hupp, J. T. J. Am. Chem. Soc. **2009**, 131, 458–460.
- (17) (a) Totten, R. K.; Weston, M. H.; Park, J. K.; Farha, O. K.; Hupp, J. T.; Nguyen, S. T. ACS Catal. 2013, 3, 1454–1459. (b) Fei, H.; Shin, J.; Meng, Y. S.; Adelhardt, M.; Sutter, J.; Meyer, K.; Cohen, S. M. J. Am. Chem. Soc. 2014, 136, 4965–4973.
- (18) Manna, K.; Zhang, T.; Lin, W. J. Am. Chem. Soc. 2014, 136, 6566-6569.
- (19) (a) Johnson, J. A.; Luo, J.; Zhang, X.; Chen, Y. S.; Morton, M. D.; Echeverria, E.; Torres, F. E.; Zhang, J. ACS Catal. 2015, 5, 5283–5291. (b) Johnson, J. A.; Zhang, X.; Reeson, T. C.; Chen, Y. S.; Zhang, J. J. Am. Chem. Soc. 2014, 136, 15881–15884. (c) Zhang, X.; Zhang, X.; Johnson, J. A.; Chen, Y. S.; Zhang, J. J. Am. Chem. Soc. 2016, 138, 8380–8383. (d) Wang, C.; Volotskova, O.; Lu, K.; Ahmad, M.; Sun, C.; Xing, L.; Lin, W. J. Am. Chem. Soc. 2014, 136, 6171–6174. (e) Park, J.; Xu, M.; Li, F.; Zhou, H. C. J. Am. Chem. Soc. 2018, 140, 5493–5499.